

一维六方压电准晶圆盘的自由振动特性研究*

张博¹ 平贺¹ 李梁娟² 王鑫鑫¹ 禹建功^{1**} 韩康乐¹

(¹ 河南理工大学机械与动力工程学院, 焦作, 454000)(² 河南理工大学数学与信息科学学院, 焦作, 454000)

摘要 压电准晶材料具有良好的压电效应和声-相耦合效应, 在传感器等压电设备中具有广泛的应用前景. 压电设备的工作性能与振动特性密切相关, 因此, 研究了一维六方压电准晶圆盘的自由振动特性. 首先, 基于三维声-相-电-弹多场耦合, 推导了一维六方压电准晶圆盘的振动力学模型, 引入矩形窗函数处理了边界问题, 使用改进的双勒让德正交多项式方法求解了动力学方程. 其次, 分析了径高比和声-相耦合效应对谐振频率的影响. 基于有限元方法, 二次开发压电准晶圆盘自由振动的仿真程序, 验证了理论计算结果. 结果表明: 与声子模态相比, 径高比 (D/H) 对相位子模态的影响更为显著, 且高阶模态对径高比 (D/H) 的变化更为敏感; 声-相耦合系数对相位子模态的影响更显著.

关键词 压电准晶, 解析积分, 双勒让德多项式, 自由振动, 声-相耦合

DOI: 10.19636/j.cnki.cjasm42-1250/o3.2025.010

0 引言

压电准晶材料内部具有相互耦合的声子场、相位子场和电场^[1], 展现出与压电晶体结构不一样的力学行为. 同时, 压电准晶具备高硬度、耐磨耐腐蚀性、高热阻、高电阻等优良性能, 在机械、化工、航空航天和压电传感器等行业具有广泛的应用前景^[2-4].

压电传感器的工作性能与结构的振动特性密切相关. 因此, 压电准晶结构的振动特性受到广泛关注. Feng 等^[5]研究了具有非完美界面准晶层合板的振动特性. Li 和 Xiao^[6]研究了一维六方压电准晶梁的振动特性. Waksmaniski 等^[7]研究了简支的一维六方准晶层状板的自由振动特性. 陈韬等^[8]推导了一维六方准晶层合简支梁自由振动与屈曲的精确解, 揭示了声-相耦合效应等对振动特性的影响规律.

压电准晶结构振动特性研究主要集中在板、梁等简单结构, 这些结构往往使用简化的梁、板理论. 对于工程中常见的圆盘结构^[9-11]振动特性的研究鲜见报道, 主要因为圆盘结构的振动特性与径向和轴

向尺寸密切相关, 简化理论造成的误差过大, 不再适用, 需对其进行三维建模求解. 此外, 压电准晶圆盘结构存在相互耦合的声子场、相位子场和电场, 大大增加了压电准晶圆盘结构振动特性的三维解的求解难度. 本文基于准晶的三维弹性理论, 使用改进的双勒让德正交多项式方法, 推导了一维六方压电准晶圆盘自由振动的三维解析解.

勒让德多项式方法是一种渐进的解析解法, 已成功应用于板、管、矩形截面杆等多种结构的振动与波动问题求解^[12-14]. 该方法主要利用其在有限区间上的正交性, 但是, 此时的积分多为数值积分, 计算比较耗时. 当使用双勒让德正交多项式求解矩形截面杆、圆盘/环等二维截面结构时, 随着多项式阶数的增加, 特征矩阵的维度快速增大, 加剧求解困难. 此外, 与压电晶体圆盘相比, 压电准晶圆盘结构的动力学控制方程增加, 也增加求解难度. 为保证求解结果收敛性, 本文推导出了数值积分的解析表达式, 快速高效地求解压电准晶圆盘的自由振动特性.

使用改进的双正交多项式方法, 研究了一维六

* 国家自然科学基金项目(12102131), 河南省高校科技创新团队项目(23IRTSTHN016), 河南理工大学青年骨干教师项目(2024XQG-16)和河南理工大学安全学部双一流建设培育项目(AQ20250711)资助.

2025-04-30 收到修改稿, 2025-05-14 网络首发.

** 通讯作者. E-mail: yuee@hpu.edu.cn.

方压电准晶圆盘的自由振动特性. 本文的主要创新工作为:(1) 使用基于解析积分的双正交多项式方法,快速高效地求解压电准晶圆盘的自由振动特性,与传统的双正交多项式相比,其效率提升高达 99%. (2) 基于有限元软件 COMSOL,二次开发了压电准晶圆盘的自由振动特性的仿真程序,模拟了其自由振动行为.

1 基本公式与求解

1.1 基本公式推导

考虑一个柱坐标系 (r, θ, z) 中的一维六方压电准晶圆盘,如图 1 所示. 准周期方向和厚度方向均为 z 轴方向,半径方向为径向(r 向),圆盘的表面和侧面为应力自由状态. 在垂直于 z 轴方向的圆盘上下表面外添加金属电极,忽略电极的边界效应,可近似认为只存在轴向电场 E_z , 因外加电极厚度较小,其质量、刚度也可以忽略不计. 假设极化方向为 z 轴方向,侧面电开路、上下表面短路,上下表面施加一外加电压 $V_0 i \omega t$, 其中, V_0 为外加电压幅值, i 为虚数单位, ω 为角频率, t 为时间变量.

根据三维电-弹理论,声子场和相位子场的几何关系为^[15,16]:

$$\left\{ \begin{array}{l} \epsilon_{\theta\theta} = \frac{1}{r} \frac{\partial u_\theta}{\partial \theta} + \frac{u_r}{r}, \quad \epsilon_{zz} = \frac{\partial u_z}{\partial z}, \quad \epsilon_{rr} = \frac{\partial u_r}{\partial r} \\ \epsilon_{r\theta} = \frac{1}{2} \left(\frac{1}{r} \frac{\partial u_r}{\partial \theta} + \frac{\partial u_\theta}{\partial r} - \frac{u_\theta}{r} \right) \\ \epsilon_{rz} = \frac{1}{2} \left(\frac{\partial u_r}{\partial z} + \frac{\partial u_z}{\partial r} \right), \quad \epsilon_{\theta z} = \frac{1}{2} \left(\frac{1}{r} \frac{\partial u_z}{\partial \theta} + \frac{\partial u_\theta}{\partial z} \right) \\ \omega_{zr} = \frac{\partial w_z}{\partial r}, \quad \omega_{z\theta} = \frac{1}{r} \frac{\partial w_z}{\partial \theta}, \quad \omega_{zz} = \frac{\partial w_z}{\partial z} \end{array} \right. \quad (1)$$

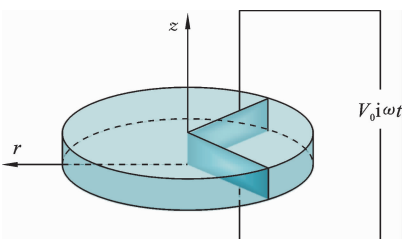


图 1 压电准晶圆盘结构示意图

Fig. 1 Schematic diagram of piezoelectric quasi-crystal discs

式中, ϵ_{ij} 和 ω_{ij} 分别代表声子场和相位子场的应变, u_i 和 w_i 分别表示声子场和相位子场的位移分量.

电势与电场关系为:

$$E_r = -\frac{\partial \phi}{\partial r}, \quad E_\theta = -\frac{\partial \phi}{r \partial \theta}, \quad E_z = -\frac{\partial \phi}{\partial z} \quad (2)$$

式中, ϕ 为电势, E_i 为电场强度.

不考虑体力,压电准晶结构的动力学控制方程为^[15,16]:

$$\frac{\partial T_{rr}}{\partial r} + \frac{1}{r} \frac{\partial T_{r\theta}}{\partial \theta} + \frac{\partial T_{rz}}{\partial z} + \frac{T_{rr} - T_{\theta\theta}}{r} = \rho \frac{\partial^2 u_r}{\partial t^2} \quad (3)$$

$$\frac{\partial T_{rz}}{\partial r} + \frac{1}{r} \frac{\partial T_{\theta z}}{\partial \theta} + \frac{\partial T_{zz}}{\partial z} + \frac{T_{rz}}{r} = \rho \frac{\partial^2 u_z}{\partial t^2} \quad (4)$$

$$\frac{\partial H_{zr}}{\partial r} + \frac{1}{r} \frac{\partial H_{z\theta}}{\partial \theta} + \frac{\partial H_{zz}}{\partial z} + \frac{H_{zr}}{r} = \rho \frac{\partial^2 w_z}{\partial t^2} \quad (5)$$

式中, T_{ij} 和 H_{ij} 分别表示声子和相位子应力, ρ 表示密度.

电场的控制方程为:

$$\frac{\partial D_r}{\partial r} + \frac{1}{r} \frac{\partial D_\theta}{\partial \theta} + \frac{\partial D_z}{\partial z} + \frac{D_r}{r} = 0 \quad (6)$$

式中, D_i 表示电位移.

根据广义的 Hook 定律,可得相应的本构方程:

$$\left\{ \begin{array}{l} T_{rr} = (C_{11} \epsilon_{rr} + C_{12} \epsilon_{\theta\theta} + C_{13} \epsilon_{zz} + R_1 \omega_{zz} - e_{31} E_z) \pi_1(r) \pi_3(z) \\ T_{\theta\theta} = (C_{12} \epsilon_{rr} + C_{11} \epsilon_{\theta\theta} + C_{13} \epsilon_{zz} + R_1 \omega_{zz} - e_{31} E_z) \\ T_{zz} = (C_{13} \epsilon_{rr} + C_{13} \epsilon_{\theta\theta} + C_{33} \epsilon_{zz} + R_2 \omega_{zz} - e_{33} E_z) \pi_1(r) \pi_3(z) \\ T_{\theta z} = T_{z\theta} = (2C_{44} \epsilon_{\theta z} + R_3 \omega_{z\theta} - e_{15} E_\theta) \pi_3(z) \\ T_{rz} = T_{zr} = (2C_{44} \epsilon_{rz} + R_3 \omega_{zr} - e_{15} E_r) \pi_1(r) \pi_3(z) \\ T_{r\theta} = T_{\theta r} = (2C_{66} \epsilon_{r\theta}) \pi_1(r) \end{array} \right. \quad (7a)$$

$$\left\{ \begin{array}{l} H_{zz} = (R_1 \epsilon_{rr} + R_1 \epsilon_{\theta\theta} + R_2 \epsilon_{zz} + K_1 \omega_{zz} - d_{33} E_z) \pi_1(r) \pi_3(z) \\ H_{z\theta} = (2R_3 \epsilon_{\theta z} + K_2 \omega_{z\theta} - d_{15} E_\theta) \pi_1(r) \pi_3(z) \\ H_{zr} = (2R_3 \epsilon_{rz} + K_2 \omega_{zr} - d_{15} E_r) \pi_1(r) \pi_3(z) \end{array} \right. \quad (7b)$$

$$\left\{ \begin{array}{l} D_z = (e_{31} \epsilon_{rr} + e_{31} \epsilon_{\theta\theta} + e_{33} \epsilon_{zz} + d_{33} \omega_{zz} + \epsilon_{33} E_z) \pi_1(r) \\ D_\theta = (2e_{15} \epsilon_{\theta z} + d_{15} \omega_{z\theta} + \epsilon_{11} E_\theta) \\ D_r = (2e_{15} \epsilon_{rz} + d_{15} \omega_{zr} + \epsilon_{11} E_r) \pi_1(r) \end{array} \right. \quad (7c)$$

式中, C_{ij} , R_i 和 K_i 分别表示声子场弹性常数、声-相耦合系数和相位子场弹性常数. e_{ij} 和 d_{ij} 分别表示声子场压电常数和相位子场压电常数, ϵ_{ij} 为介电常数.

在上式中引入了 r 向和 z 向的矩形窗函数,其

具体表述为：

$$\pi_1(r) = \begin{cases} 1, & 0 \leq r \leq R \\ 0, & \text{其他} \end{cases}, \quad \pi_3(z) = \begin{cases} 1, & 0 \leq z \leq H \\ 0, & \text{其他} \end{cases} \quad (8)$$

矩形窗函数的导数在数学上是由两个冲激函数组成的符号函数^[17], $\pi_1(r)$ 对变量 r 的导数为 $\delta(r) - \delta(r-R)$, $\pi_3(z)$ 对变量 z 的导数为 $\delta(z) - \delta(z-H)$. 通过带入 $\pi_1(r)$ 和 $\pi_3(z)$, 声子场和相位子场边界^[14]自由的初始条件可以自动带入到本构方程中, 即:

$$\begin{cases} \left. \begin{aligned} T_{rz} |_{z=0, H} = T_{zz} |_{z=0, H} = 0 \\ T_{rz} |_{r=0, R} = T_{zz} |_{r=0, R} = 0 \end{aligned} \right\} \text{自由} \\ D_r |_{r=R} = 0 \quad \text{开路} \\ \left. \begin{aligned} \phi |_{z=0} = 0, \quad \phi |_{z=H} = 0 \end{aligned} \right\} \text{短路} \end{cases} \quad (9)$$

由于压电圆盘作轴对称振动, 所以振动与方位角 θ 无关^[9], 即 $\left(\frac{\partial}{\partial \theta} = 0, u_\theta = 0\right)$, 一维六方压电准晶圆盘的声子场和相位子场的位移分量及电势可以写为:

$$\begin{cases} u_r = U(r, z)e^{i\omega t}, & u_z = W(r, z)e^{i\omega t} \\ \omega_z = \gamma(r, z)e^{i\omega t}, & \phi = \Phi(r, z)e^{i\omega t} \end{cases} \quad (10)$$

式中, $U(r, z)$ 和 $W(r, z)$ 分别代表 r 和 z 方向的声子位移分量的振幅, $\gamma(r, z)$ 代表 z 向的相位子位移分量的振幅, $\Phi(r, z)$ 代表电势的振幅.

将本构方程、几何关系、声子和相位子位移及电势带入到振动控制方程中, 可得相应的振动微分控制方程:

$$\begin{aligned} \pi_1(r)\pi_3(z) & \left(C_{11}U_{,rr} + C_{13}W_{,rz} + R_1\gamma_{,rz} + e_{31}\Phi_{,rz} + \right. \\ & C_{44}U_{,zz} + C_{44}W_{,rz} + R_3\gamma_{,rz} + e_{15}\Phi_{,rz} + \frac{C_{11}}{r}U_{,r} - \\ & \left. \frac{C_{11}}{r^2}U \right) + \pi'_1(r)\pi_3(z) \left(C_{11}U_{,r} + \frac{C_{12}}{r}U + C_{13}W_{,z} \right. \\ & \left. + R_1\gamma_{,z} + e_{31}\Phi_{,z} \right) + \pi_1(r)\pi'_3(z) (C_{44}U_{,z} + C_{44} \\ & W_{,r} + R_3\gamma_{,r} + e_{15}\Phi_{,r}) = -\rho\omega^2\pi_1(r)\pi_3(z)U \end{aligned} \quad (11)$$

$$\begin{aligned} \pi_1(r)\pi_3(z) & \left[C_{44}(U_{,rz} + W_{,rr}) + R_3\gamma_{,rr} + e_{15}\Phi_{,rr} + C_{13} \right. \\ & \left. U_{,rz} + \frac{C_{13}}{r}U_{,z} + C_{33}W_{,zz} + R_2\gamma_{,zz} + e_{33}\Phi_{,zz} + \right. \end{aligned}$$

$$\begin{aligned} & \left. \frac{C_{44}}{r}U_{,z} + \frac{C_{44}}{r}W_{,r} + \frac{R_3}{r}\gamma_{,r} + \frac{e_{15}}{r}\Phi_{,r} \right] + \\ & \pi'_1(r)\pi_3(z) [C_{44}(U_{,r} + W_{,r}) + R_3\gamma_{,r} + e_{15}\Phi_{,r}] \\ & + \pi_1(r)\pi'_3(z) \left(C_{13}U_{,r} + \frac{C_{13}}{r}U + C_{33}W_{,z} + R_2\gamma_{,z} \right. \\ & \left. + e_{33}\Phi_{,z} \right) = -\rho\omega^2\pi_1(r)\pi_3(z)W \end{aligned} \quad (12)$$

$$\begin{aligned} \pi_1(r)\pi_3(z) & \left(R_3U_{,rz} + R_3W_{,rr} + K_2\gamma_{,rr} + d_{15}\Phi_{,rr} R_1U_{,rz} \right. \\ & \left. + \frac{R_1}{r}U_{,z} + R_2W_{,zz} + K_1\gamma_{,zz} + d_{33}\Phi_{,zz} \frac{R_3}{r}U_{,z} + \right. \\ & \left. \frac{R_3}{r}W_{,r} + \frac{K_2}{r}\gamma_{,r} + \frac{d_{15}}{r}\Phi_{,r} \right) + \pi'_1(r)\pi_3(z) (R_3U_{,z} + \\ & R_3W_{,r} + K_2\gamma_{,r} + d_{15}\Phi_{,r}) + \pi_1(r)\pi'_3(z) \left(R_1U_{,r} + \right. \\ & \left. \frac{R_1}{r}U + R_2W_{,z} + K_1\gamma_{,z} + d_{33}\Phi_{,z} \right) \\ & = -\rho\omega^2\pi_1(r)\pi_3(z)\gamma \end{aligned} \quad (13)$$

$$\begin{aligned} \pi_1(r)\pi_3(z) & \left(e_{15}U_{,rz} + e_{15}W_{,rr} + d_{15}\gamma_{,rr} - \epsilon_{11}\Phi_{,rr} + e_{31} \right. \\ & \left. U_{,rz} + \frac{e_{31}}{r}U_{,z} + e_{33}W_{,zz} + d_{33}\gamma_{,zz} - \epsilon_{33}\Phi_{,zz} + \frac{e_{15}}{r} \right. \\ & \left. U_{,z} + \frac{e_{15}}{r}W_{,r} + \frac{d_{15}}{r}\gamma_{,r} - \frac{\epsilon_{11}}{r}\Phi_{,r} \right) + \pi'_1(r)\pi_3(z) \\ & (e_{15}U_{,z} + e_{15}W_{,r} + d_{15}\gamma_{,r} - \epsilon_{11}\Phi_{,r}) = 0 \end{aligned} \quad (14)$$

为求解耦合方程式(14), 将振幅展开成双 Legendre 正交多项式级数的形式, 表示为:

$$\begin{cases} U(r, z) = \sum_{mm} P_{m, 2n+1}^1 Q_m(r) Q_{2n+1}(z) \\ W(r, z) = \sum_{mm} P_{m, 2n+1}^2 Q_m(r) Q_{2n+1}(z) \\ \gamma(r, z) = \sum_{mm} P_{m, 2n+1}^3 Q_m(r) Q_{2n+1}(z) \\ \Phi(r, z) = [V_0 z/H + z(z-H)] \cdot \\ \sum_{mm} r_{m, 2n+1} Q_m(r) Q_{2n+1}(z) \end{cases} \quad (15)$$

式中, $P_{m, 2n+1}^1, P_{m, 2n+1}^2, P_{m, 2n+1}^3, r_{m, 2n+1}$ 是多项式的待定系数.

$$\begin{cases} Q_m(r) = \sqrt{\frac{2m+1}{R}} P_m\left(\frac{2r}{R} - 1\right) \\ Q_n(z) = \sqrt{\frac{2n+1}{H}} P_n\left(\frac{2z}{H} - 1\right) \end{cases} \quad (16)$$

式中, P_m 和 P_n 分别表示第 m 阶和 n 阶勒让德多

项式. 理论上, m 和 n 从 0 变化到 ∞ , 当 m 和 n 取到有限值 M 和 N 时, 求和多项式(15)已经收敛, 更高阶的项可以认为是高阶无穷小量, 从而忽略不计.

将式(15)和(16)代入式(11)到(14), 用 $Q_k(r)$ $Q_l(z)$ 乘等式的两边, k 从 0 变化到 M , l 从 0 变化到 N , 对 z 从 0 到 H , r 从 0 到 R 积分, 利用其正交特性, 可得下式:

$$\begin{cases} A1P_{m,2n+1}^1 + B1P_{m,2n+1}^2 + C1P_{m,2n+1}^3 + D1r_{m,2n+1} + f_1V_0 = -\omega^2 M1P_{m,2n+1}^1 \\ A2P_{m,2n+1}^1 + B2P_{m,2n+1}^2 + C2P_{m,2n+1}^3 + D2r_{m,2n+1} + f_2V_0 = -\omega^2 M2P_{m,2n+1}^2 \\ A3P_{m,2n+1}^1 + B3P_{m,2n+1}^2 + C3P_{m,2n+1}^3 + D3r_{m,2n+1} + f_3V_0 = -\omega^2 M3P_{m,2n+1}^3 \\ A4P_{m,2n+1}^1 + B4P_{m,2n+1}^2 + C4P_{m,2n+1}^3 + D4r_{m,2n+1} + f_4V_0 = 0 \end{cases} \quad (17)$$

其中, $A1, A2, A3, A4, B1, B2, B3, B4, C1, C2, C3, C4, D1, D2, D3, D4, M1, M2, M3$ 都是 $(M+1) \times (N+1)$ 阶矩阵; f_1, f_2, f_3 以及 $P_{m,2n+1}^1, P_{m,2n+1}^2, P_{m,2n+1}^3, r_{m,2n+1}$ 为 $(M+1) \times (N+1)$ 阶列向量.

为了便于计算, 取

$$ABC = \begin{bmatrix} A1 & B1 & C1 \\ A2 & B2 & C2 \\ A3 & B3 & C3 \end{bmatrix}, \quad DD = \begin{bmatrix} D1 \\ D2 \\ D3 \end{bmatrix}$$

$$P_{m,n} = \begin{bmatrix} P_{m,2n+1}^1 \\ P_{m,2n+1}^2 \\ P_{m,2n+1}^3 \end{bmatrix}$$

$$ABC4 = [A4 \quad B4 \quad C4], \quad MM = \begin{bmatrix} M1 & & \\ & M2 & \\ & & M3 \end{bmatrix}$$

$$f_{1,2,3} = \begin{bmatrix} f_1 \\ f_2 \\ f_3 \end{bmatrix}$$

则方程(17)可以简化为:

$$\begin{bmatrix} ABC & DD \\ ABC4 & D4 \end{bmatrix} \begin{bmatrix} P_{m,n} \\ r_{m,2n+1} \end{bmatrix} + \begin{bmatrix} f_{1,2,3} \\ f_4 \end{bmatrix} V_0 = -\omega^2 \begin{bmatrix} MM & 0 \\ 0 & 0 \end{bmatrix} \begin{bmatrix} P_{m,n} \\ r_{m,2n+1} \end{bmatrix} \quad (18)$$

与此同时, 求出式(17)中的 $r_{m,2n+1}$ 并代入(18),

可以得到:

$$[ABCD + \omega^2 MM]P_{m,n} = C_f V_0 \quad (19)$$

其中, $ABCD = ABC - DD(D4)^{-1}ABC4$, $C_f = DD(D4)^{-1}f_4 - f_{1,2,3}$.

由压电材料谐响应特性可知, 谐振频率点处的阻抗很小, 即此时模型电极间电势很小, 近似为零^[18]. 将 $V_0 = 0$ 代入式(19), 即可得到求解谐振频率的特征方程:

$$(MM)^{-1}ABCDP_{m,n} = -\omega^2 P_{m,n} \quad (20)$$

利用特征矩阵求特征值, 可以得到角频率 ω .

1.2 解析积分

求解式(20)需要涉及大量数值积分, 这些积分比较费时, 导致计算效率降低. 此外, 与晶体圆盘相比, 压电准晶圆盘所涉及的物理场更多、更复杂, 计算耗时会更长. 推导出这些积分的解析表达式能使程序计算时间大大缩减. 上述过程涉及到五种形式数值积分归纳如下:

$$\begin{cases} I_1 = \int_{-1}^1 t^a P_n(t) P_m(t) dt \\ I_2 = \int_{-1}^1 t^a P_n(t) \frac{d}{dt} P_m(t) dt \\ I_3 = \int_{-1}^1 t^a P_n(t) \frac{d^2}{dt^2} P_m(t) dt \\ I_4 = \int_{-1}^1 t^a P_n(t) P_m(t) \frac{d}{dt} [h(t+1) - h(t-1)] dt \\ I_5 = \int_{-1}^1 t^a P_n(t) \frac{d}{dt} P_m(t) \frac{d}{dt} [h(t+1) - h(t-1)] dt \end{cases} \quad (21)$$

利用 Heaviside 函数自身特性和多项式的正交性, 可以得到:

(1) 当 $a+m \geq n$ 和 $a+m-n =$ 偶数时, 令 $p = \frac{m+a-n-2s}{2}$.

$$I_1 = \sum_{s=0}^{\lfloor \frac{m}{2} \rfloor} (-1)^s \frac{(2m-2s)!}{2^m s! (m-s)! (m-2s)!} \cdot \frac{2^{n+1} (n+2p)! (n+p)!}{p! (2n+2p+1)!}$$

当 a, m, n 取其他值时, $I_1 = 0$.

(2) 当 $a+m-1 \geq n$ 和 $a+m-n-1 =$ 偶数时,

令 $p = \frac{m+a-n-2s-1}{2}$.

$$I_2 = \sum_{s=0}^{\lfloor \frac{m}{2} \rfloor} (-1)^s \frac{(2m-2s)!}{2^m s!(m-s)!(m-2s)!} \cdot \frac{2^{n+1}(n+2p)!(n+p)!}{p!(2n+2p+1)!}$$

当 a, m, n 取其他值时, $I_2 = 0$.

(3) 当 $a+m-2 \geq n$ 和 $a+m-n-2 = \text{偶数}$ 时,

$$\text{令 } p = \frac{m+a-n-2s-2}{2}$$

$$I_3 = \sum_{s=0}^{\lfloor \frac{m}{2} \rfloor} (-1)^s \frac{(2m-2s)!}{2^m s!(m-s)!(m-2s)!} \cdot \frac{2^{n+1}(n+2p)!(n+p)!}{p!(2n+2p+1)!}$$

当 a, m, n 取其他值时, $I_3 = 0$.

$$\begin{cases} I_4 = (-1)^a P_n(-1) P_m(-1) - P_n(1) P_m(1) \\ I_5 = (-1)^a P_n(-1) \left[\frac{d}{dt} P_m(t) \right]_{t=-1} - \\ P_n(1) \left[\frac{d}{dt} P_m(t) \right]_{t=1} \end{cases} \quad (22)$$

2 有限元仿真

由于压电准晶存在复杂的声-相耦合和压电效应, 目前鲜见关于一维六方准晶圆盘的振动特性的报道. 为了验证程序结果的正确性, 对纳米准晶圆盘

振动进行有限元仿真. 由于现有的有限元软件不附带准晶相关模块. 因此, 需要根据现有模块进行二次开发, 仿真准晶圆盘的自由振动.

COMSOL 软件是一个多物理场建模及仿真软件, 它常用于处理各种复杂的工程和科学问题. 软件包含自定义 PDE 模块供用户进行自主开发来满足需要. 本文研究对象为圆盘, 更适应柱坐标体系. 打开 COMSOL, 在模型向导中选择“二维轴对称”这一空间维度, 随后在界面左侧选择物理场“数学”接口分支下的“偏微分方程”接口, 并在此分支下选择“系数型偏微分方程”接口, 特征方程的形式为:

$$\begin{cases} \lambda^2 e_a u - \lambda d_a u + \nabla \cdot (-c \nabla u - \alpha u + \gamma) + \\ \beta \cdot \nabla u + a u = f \\ u = [u_1, u_2, u_3, u_4]^T, \quad \nabla = \left[\frac{\partial}{\partial r}, \frac{\partial}{\partial z} \right] \end{cases} \quad (23)$$

式中, λ 为特征值, $e_a, d_a, c, \alpha, \gamma, \beta, a$ 均为根据控制方程确定的系数矩阵, 分别为质量系数、阻尼或质量系数、扩散系数、守恒通量对流系数、守恒通量源、对流系数和吸收系数; f 为源项, 是根据边界条件确定的表达式, u_1, u_2, u_3, u_4 分别对应 u_r, u_z, ω_z, ϕ . 将前文所推公式与这些系数矩阵的形式相比较, 为零的系数矩阵不再列出, 材料参数的输入参考表 1, 能得出系数矩阵如下所示:

$$c = \begin{bmatrix} \begin{bmatrix} -C_{11} & 0 \\ 0 & -C_{44} \end{bmatrix} & \begin{bmatrix} 0 & -C_{13} \\ -C_{44} & 0 \end{bmatrix} & \begin{bmatrix} 0 & -R_1 \\ -R_3 & 0 \end{bmatrix} & \begin{bmatrix} 0 & -e_{31} \\ -e_{15} & 0 \end{bmatrix} \\ \begin{bmatrix} 0 & -C_{44} \\ -C_{13} & 0 \end{bmatrix} & \begin{bmatrix} -C_{44} & 0 \\ 0 & -C_{33} \end{bmatrix} & \begin{bmatrix} -R_3 & 0 \\ 0 & -R_2 \end{bmatrix} & \begin{bmatrix} -e_{15} & 0 \\ 0 & -e_{33} \end{bmatrix} \\ \begin{bmatrix} 0 & -R_3 \\ -R_1 & 0 \end{bmatrix} & \begin{bmatrix} -R_3 & 0 \\ 0 & -R_2 \end{bmatrix} & \begin{bmatrix} -K_2 & 0 \\ 0 & -K_1 \end{bmatrix} & \begin{bmatrix} -d_{15} & 0 \\ 0 & -d_{33} \end{bmatrix} \\ \begin{bmatrix} 0 & -e_{15} \\ -e_{31} & 0 \end{bmatrix} & \begin{bmatrix} -e_{15} & 0 \\ 0 & -e_{33} \end{bmatrix} & \begin{bmatrix} -d_{15} & 0 \\ 0 & -d_{33} \end{bmatrix} & \begin{bmatrix} \epsilon_{11} & 0 \\ 0 & \epsilon_{33} \end{bmatrix} \end{bmatrix},$$

$$\alpha = \frac{1}{r} \begin{bmatrix} \begin{bmatrix} -C_{12} \\ 0 \end{bmatrix} & \begin{bmatrix} 0 \\ 0 \end{bmatrix} & \begin{bmatrix} 0 \\ 0 \end{bmatrix} & \begin{bmatrix} 0 \\ 0 \end{bmatrix} \\ \begin{bmatrix} 0 \\ -C_{13} \end{bmatrix} & \begin{bmatrix} 0 \\ 0 \end{bmatrix} & \begin{bmatrix} 0 \\ 0 \end{bmatrix} & \begin{bmatrix} 0 \\ 0 \end{bmatrix} \\ \begin{bmatrix} 0 \\ -R_1 \end{bmatrix} & \begin{bmatrix} 0 \\ 0 \end{bmatrix} & \begin{bmatrix} 0 \\ 0 \end{bmatrix} & \begin{bmatrix} 0 \\ 0 \end{bmatrix} \\ \begin{bmatrix} 0 \\ -e_{31} \end{bmatrix} & \begin{bmatrix} 0 \\ 0 \end{bmatrix} & \begin{bmatrix} 0 \\ 0 \end{bmatrix} & \begin{bmatrix} 0 \\ 0 \end{bmatrix} \end{bmatrix},$$

$$\beta = \frac{1}{r} \begin{bmatrix} \begin{bmatrix} C_{11} - C_{12} \\ 0 \end{bmatrix} & \begin{bmatrix} 0 \\ 0 \end{bmatrix} & \begin{bmatrix} 0 \\ 0 \end{bmatrix} & \begin{bmatrix} 0 \\ 0 \end{bmatrix} \\ \begin{bmatrix} 0 \\ C_{44} \end{bmatrix} & \begin{bmatrix} C_{44} \\ 0 \end{bmatrix} & \begin{bmatrix} R_3 \\ 0 \end{bmatrix} & \begin{bmatrix} e_{15} \\ 0 \end{bmatrix} \\ \begin{bmatrix} 0 \\ R_3 \end{bmatrix} & \begin{bmatrix} R_3 \\ 0 \end{bmatrix} & \begin{bmatrix} K_2 \\ 0 \end{bmatrix} & \begin{bmatrix} d_{15} \\ 0 \end{bmatrix} \\ \begin{bmatrix} 0 \\ e_{15} \end{bmatrix} & \begin{bmatrix} e_{15} \\ 0 \end{bmatrix} & \begin{bmatrix} d_{15} \\ 0 \end{bmatrix} & \begin{bmatrix} -\epsilon_{11} \\ 0 \end{bmatrix} \end{bmatrix},$$

$$a = \frac{1}{r^2} \begin{bmatrix} C_{12} - C_{11} & 0 & 0 & 0 \\ 0 & 0 & 0 & 0 \\ 0 & 0 & 0 & 0 \\ 0 & 0 & 0 & 0 \end{bmatrix}, \quad e_a = \begin{bmatrix} \rho & 0 & 0 & 0 \\ 0 & \rho & 0 & 0 \\ 0 & 0 & \rho & 0 \\ 0 & 0 & 0 & 0 \end{bmatrix} \quad (24)$$

构建几何模型,设置半径 $R=10$ mm, 厚度 $H=2$ mm, 如图 2 所示. 设置压电准晶圆盘的电边界条件为上下表面短路, 实现方法为在“系数型偏微分方程”接口添加“狄利克雷边界条件”, 指定 u_4 的

等于 0, 来保证圆盘上下表面零电势的电边界条件. 机械边界条件为自由边界因此不需要进行额外的设置. 然后, 划分自由四边形网格并细化, 构建几何体对象. 最后, 添加研究为“特征值”, 特征值数量设置为“20”即可满足需求, 其余研究设置依照默认设置, 在结果的表格设置中输入使特征值结果除以 2π 的表达式, 输出即可得到特征频率, 并与程序计算结果作对比, 如表 2 所示. 可以看到, 两者结果一致.

表 1 一维六方压电准晶材料常数

Table 1 Material constants of one-dimensional hexagonal piezoelectric quasi-crystal

| | | | | | | | | | |
|----------|----------|----------|----------|----------|----------|-----------------|-----------------|--------|--------|
| C_{11} | C_{12} | C_{13} | C_{33} | C_{44} | C_{66} | K_1 | K_2 | R_1 | R_2 |
| 234.33 | 57.41 | 66.63 | 232.22 | 70.19 | 88.46 | 12.2 | 2.4 | 0.8846 | 0.8846 |
| R_3 | e_{31} | e_{33} | e_{15} | d_{15} | d_{33} | ϵ_{11} | ϵ_{33} | ρ | |
| 0.8846 | -4.4 | 18.6 | 11.6 | 1.16 | 1.86 | 5 | 10 | 4.186 | |

单位: C_{ij} (GPa), K_i (10^{10} N/m²), R_i (10^9 N/m²), e_{ij} (C/m²), d_{ij} (C/m²), ϵ_{ij} (10^{-9} C²/(N · m²)), ρ (10^3 kg/m³).

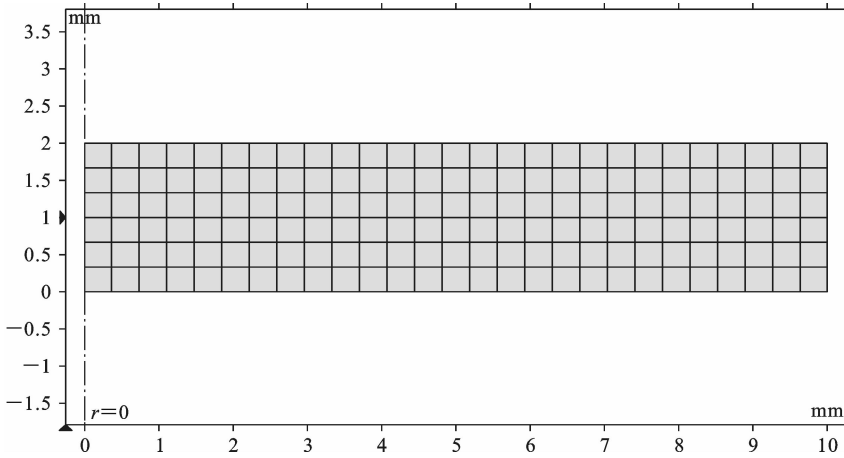


图 2 压电准晶圆盘的有限元软件轴对称建模

Fig. 2 Finite element software axisymmetric modelling of piezoelectric quasi-crystal discs

表 2 声子和相位子前四阶模式的谐振频率

Table 2 The resonant frequency of the first four phonon and phason modes

| | 程序计算结果 | 有限元仿真结果 | 误差计算 | |
|-------|--------|---------|-------------|---------|
| 声子模式 | 1 | 224573 | 224494.0372 | 0.035% |
| | 2 | 609477 | 610173.8385 | -0.114% |
| | 3 | 962919 | 962880.0719 | 0.004% |
| | 4 | 1289290 | 1290164.222 | -0.068% |
| 相位子模式 | 1 | 1349860 | 1351020.178 | -0.086% |
| | 2 | 1357750 | 1357452.073 | 0.022% |
| | 3 | 1376120 | 1376893.512 | -0.056% |
| | 4 | 1404520 | 1405564.604 | -0.074% |

3 数值结果

根据上述理论推导, 编写相应的计算机程序, 得到一维六方压电准晶圆盘的谐振频率. 除特殊说明之外, 圆盘的半径为 $R=10$ mm, 高为 $H=2$ mm.

1.3 收敛性分析

双勒让德多项式方法是一种渐进解析方法, 其结果的收敛性取决于多项式的阶数 M 和 N . 为了验证结果的收敛性, 当双勒让德多项式阶数 M 和 N 变化时, 计算得到一维六方压电准晶圆盘的前四阶

谐振频率. 这里, 对计算结果进行归一化处理, 如下所示^[19]:

$$\Omega = 2Hf \sqrt{\frac{\rho}{C_{44}}} \quad (25)$$

其中, Ω 为归一化频率, f 为谐振频率, 得到的归一化频率如表 3 和表 4 所示.

表 3 当 M 和 N 变化时, 前四阶声子模态的归一化频率

Table 3 Normalized frequencies of the first four orders of phonon modes as M and N vary

| | 第一阶 | 第二阶 | 第三阶 | 第四阶 |
|----------|------------|------------|------------|------------|
| $M=N=3$ | 0.21936486 | 0.59495032 | 1.07453861 | 1.31854325 |
| $M=N=4$ | 0.21936291 | 0.59569855 | 0.94468868 | 1.31854325 |
| $M=N=5$ | 0.21936291 | 0.59533127 | 0.94420809 | 1.28311471 |
| $M=N=6$ | 0.21936291 | 0.59533811 | 0.94057147 | 1.27289738 |
| $M=N=7$ | 0.21936291 | 0.59533713 | 0.94061151 | 1.25995478 |
| $M=N=8$ | 0.21936291 | 0.59533713 | 0.94057928 | 1.25969105 |
| $M=N=9$ | 0.21936291 | 0.59533713 | 0.94057928 | 1.25938824 |
| $M=N=10$ | 0.21936291 | 0.59533713 | 0.94057928 | 1.25937847 |
| $M=N=11$ | 0.21936291 | 0.59533713 | 0.94057928 | 1.25937847 |

表 4 当 M 和 N 变化时, 前四阶相位子模态的归一化频率

Table 4 Normalized frequencies of the first four orders of phason modes as M and N vary

| | 第一阶 | 第二阶 | 第三阶 | 第四阶 |
|----------|------------|------------|------------|------------|
| $M=N=3$ | 1.32625997 | 1.35082649 | 1.41658466 | 1.51686295 |
| $M=N=4$ | 1.32625020 | 1.34446752 | 1.39571045 | 1.48692403 |
| $M=N=5$ | 1.31854325 | 1.32625020 | 1.34432100 | 1.37358593 |
| $M=N=6$ | 1.31854325 | 1.32625020 | 1.34420378 | 1.37290217 |
| $M=N=7$ | 1.31854325 | 1.32625020 | 1.34419402 | 1.37197421 |
| $M=N=8$ | 1.31854325 | 1.32625020 | 1.34419402 | 1.37194490 |
| $M=N=9$ | 1.31854325 | 1.32625020 | 1.34419402 | 1.37193514 |
| $M=N=10$ | 1.31854325 | 1.32625020 | 1.34419402 | 1.37193514 |
| $M=N=11$ | 1.31854325 | 1.32625020 | 1.34419402 | 1.37193514 |

可以看到, 随着双勒让德多项式阶数 (M, N) 的增大, 一维六方压电准晶圆盘的归一化频率逐步趋向收敛. 当 $M=N=10$ 时, 声子场和相位子场前四阶模态已经全部收敛. 此外, 各个模态的收敛速度不一致, 比如, 当 $M=N=9$ 时, 声子场前三阶模态收敛, 相位子场则是前四阶模态已经收敛. 为了保证后面结果的收敛性, 本文令 $M=N=10$.

3.2 计算效率

如上所述, 推导出所有数值积分的解析表达式, 可提高其计算效率. 因此, 这一小节分别对比了数值

积分和解析积分所用时间. 当 M 和 N 取不同值时, 表 5 给出了两种计算方法所需时间. 本次计算所使用的电脑配置 CPU 为: 11th Gen Intel (R) Core (TM) i5-1135G7 @ 2.40 GHz, 2.42 GHz. 可以看到, 使用解析积分, 能够大大提高计算效率, 计算效率的提高可达 99% 以上. 此外, 对于数值积分, 阶数较大时, 需要几天甚至更长时间, 比如, 当 $M=N=7$ 时, 计算时间超过 3 天.

3.3 径高比 (D/H) 对归一化频率的影响

这一小节分析压电圆盘的径高比 (D/H) 变化对

表5 解析积分与传统数值积分的计算时间对比

Table 5 Comparison of computation time between analytic integration and conventional integration

| $M=N$ | 解析法(s) | 传统法(s) | 计算效率 |
|-------|--------|---------|---------|
| 4 | 1.578 | 17845.6 | 99.991% |
| 5 | 3.406 | 48673.4 | 99.993% |
| 6 | 6.704 | 113970 | 99.994% |
| 7 | 16.5 | 323893 | 99.995% |
| 8 | 27.359 | / | / |
| 9 | 48.329 | / | / |
| 10 | 76.001 | / | / |

归一化频率的影响,其中 D 为圆盘直径, H 为圆盘厚度. 首先,令 $D=20$ mm 保持不变, H 逐渐减小,分别计算得到前四阶声子模态和前四阶相位子模态的归一化频率如表6和表7所示.

这里定义归一化频率的变化率 η_n 如下所示:

$$\eta_n = \frac{\Omega_n - \Omega_1}{\Omega_1} \times 100\% \quad (26)$$

其中, Ω_n 表示径高比(D/H)值为 n 时归一化频率, Ω_1 表示径高比(D/H)值为1时归一化频率.

由表6和表7数据变化可以看出,随着径高比(D/H)的增大,声子和相位子模态的归一化频率均增大,且相应的变化率显著增大.二者对比来看,相

表6 当径高比(D/H)变化时,前四阶声子模态的归一化频率

Table 6 Normalized frequencies of the first four orders of phonon modes as diameter-to-height ratio vary

| | | 第一阶 | 第二阶 | 第三阶 | 第四阶 |
|---------|------------|------------|------------|------------|------------|
| $D/H=1$ | Ω_1 | 0.16224160 | 0.20367061 | 0.24245250 | 0.31762801 |
| | η_1 | 0 | 0 | 0 | 0 |
| $D/H=3$ | Ω_3 | 0.21715338 | 0.45111261 | 0.49635115 | 0.55282680 |
| | η_3 | 33.846% | 121.491% | 104.721% | 74.049% |
| $D/H=5$ | Ω_5 | 0.21877390 | 0.58139820 | 0.76046908 | 0.81278160 |
| | η_5 | 34.845% | 185.460% | 213.657% | 155.891% |
| $D/H=7$ | Ω_7 | 0.21916462 | 0.59164971 | 0.91345843 | 1.05821628 |
| | η_7 | 35.085% | 190.493% | 276.758% | 233.162% |
| $D/H=9$ | Ω_9 | 0.21931895 | 0.59458402 | 0.93603130 | 1.23689254 |
| | η_9 | 35.180% | 191.934% | 286.068% | 289.415% |

表7 当径高比(D/H)变化时,前四阶相位子模态的归一化频率

Table 7 Normalized frequencies of the first four orders of phason modes as diameter-to-height ratio vary

| | | 第一阶 | 第二阶 | 第三阶 | 第四阶 |
|---------|------------|------------|------------|------------|------------|
| $D/H=1$ | Ω_1 | 0.13185335 | 0.19424352 | 0.29282120 | 0.39583550 |
| | η_1 | 0 | 0 | 0 | 0 |
| $D/H=3$ | Ω_3 | 0.39556200 | 0.42052901 | 0.47409476 | 0.54782949 |
| | η_3 | 200.001% | 116.496% | 61.906% | 38.398% |
| $D/H=5$ | Ω_5 | 0.65927162 | 0.67454682 | 0.70918610 | 0.76046908 |
| | η_5 | 400.004% | 247.269% | 142.191% | 92.117% |
| $D/H=7$ | Ω_7 | 0.92298223 | 0.93395364 | 0.95927035 | 0.99776213 |
| | η_7 | 600.007% | 380.816% | 227.596% | 152.065% |
| $D/H=9$ | Ω_9 | 1.18669478 | 1.19524178 | 1.21512943 | 1.24575211 |
| | η_9 | 800.011% | 515.332% | 314.973% | 214.715% |

位子模式的归一化频率变化相对较大,尤其是在高 D/H 值时,变化率显著;而声子模式的归一化频率变化率相对较小,且逐渐趋于稳定.此外,随着径高比 (D/H) 的逐渐增大,声子和相位子模式各阶数的归一化频率呈现不均匀的上升趋势,声子模式下的归一化频率上升变化率逐步放缓,但相位子模式下的归一化频率上升变化率速度迅速增大.综合来看,与声子模式相比,径高比 (D/H) 对相位子模式的影响更为显著,且高阶模式对径高比 (D/H) 的变化更为敏感.

当径高比变化时,图 3 给出了第一阶声子模式和相位子模式的归一化频率.其他模式的变化趋势

相似,不再给出图示.声子模式和相位子模式的归一化频率均随着径高比 (D/H) 的增大而增大,但是声子模式出现明显拐点,相位子模式线性增加.这是因为声子模式的振动模式受径高比变化的影响,在径高比达到某个值时触发振动模式的转变^[20].相位子模式的线性增加表明其动力学受均匀应变场支配,其归一化频率正比于相位子波速与相位子波矢的乘积.其中,相位子波速为根号下相位子弹性常数与准晶体密度的比值,在本文中为常量,相位子波矢在本文中可等效为圆盘厚度的倒数,因此,相位子模式的归一化频率随径高比线性增加^[15].

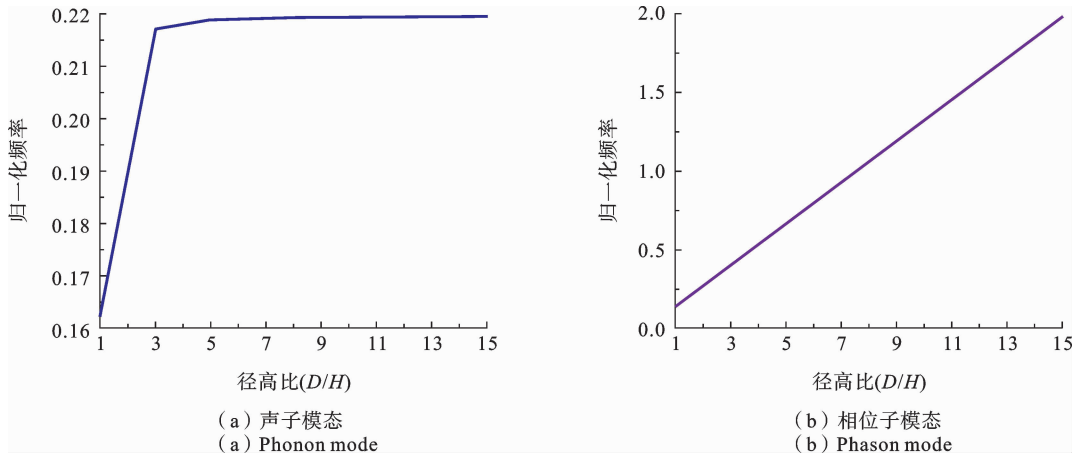


图 3 不同径高比 (D/H) 下第一阶声子和相位子模式的归一化频率

Fig. 3 Normalized frequencies of the first phonon and phason mode with different diameter-to-height ratio

3.4 声-相耦合效应对归一化频率的影响

接下来,分析声-相耦合效应对一维六方压电

准晶圆盘归一化频率的影响.当声-相耦合系数变化时,第一阶声子模式和相位子模式的归一化频率

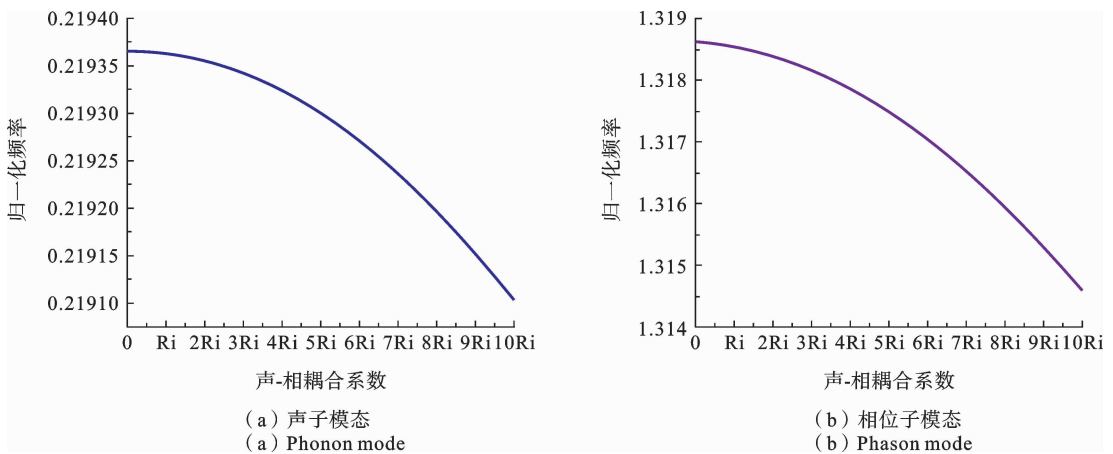


图 4 不同声-相耦合系数下第一阶声子和相位子模式的归一化频率

Fig. 4 Normalized frequencies of first phonon and phason mode with different phonon-phason coupling coefficients

如图4所示.其他模态具有相同的变化趋势,不再给出图示.可以看到,声子模态和相位子模态的归一化频率随着声-相耦合系数的增大而减小,且斜率逐渐增加,这是由于耦合效应导致系统发生动力学软化和能量再分配.当耦合强度接近临界值时,系统的动力学响应表现出显著的非线性特征,此时高阶非线性耦合项影响变大,并主导频率重整化过程^[21].此外,与声子模态对比,声-相耦合效应对相位子模态的影响更为显著,这是因为相位子因依赖长程几何约束和高维投影,其模态对局域扰动更敏感^[22].

4 结论

本文基于解析的双勒让德正交多项式方法,研究了一维六方压电准晶圆盘结构的自由振动特性,分析了声-相耦合效应和径高比对振动特性的影响.根据上述数值结果,可得如下的主要结论:

- (1) 与传统的双正交多项式方法相比,解析的双正交多项式方法的计算效率显著提高,提高率可高达99%.
- (2) 开发的有限元模型结果与理论计算结果一致.
- (3) 与声子模态相比,径高比(D/H)对相位子模态的影响更为显著,且高阶模态对径高比(D/H)的变化更为敏感.
- (4) 声-相耦合效应致使声子模态和相位子模态的归一化频率减小,并且对相位子模态的影响更为显著.

参考文献

- [1] Li Y D, Bao R, Chen W. Axial shear fracture of a transversely isotropic piezoelectric quasicrystal cylinder: Which field (phonon or phason) has more contribution[J]. *European Journal of Mechanics-A/Solids*, 2018, 71: 179-186.
- [2] 张炳彩, 丁生虎. 压电效应下一维六方准晶双材料孔边裂纹的反平面问题研究[J]. *力学季刊*, 2022, 43(3): 640-650. (Zhang B C, Ding S H. On the anti-plane problem of a crack emanating from a hole in one-dimensional hexagonal quasicrystal bi-material with piezoelectric effect [J]. *Chinese Quarterly of Mechanics*, 2022, 43(3): 640-650. (in Chinese))
- [3] 郭怀民, 赵国忠, 刘官厅, 姜丽娟. 含唇口次生两不对称裂纹的一维六方压电准晶体的反平面剪切问题[J]. *固体力学学报*, 2024, 45(01): 123-134. (Guo H M, Zhao G Z, Liu G T, Jiang L J. The anti-plane shear problem of a lip shaped orifice with two asymmetric edge rips in the one-dimensional hexagonal piezoelectric quasicrystal material [J]. *Chinese Journal of Solid Mechanics*, 2024, 45(01): 123-134. (in Chinese))
- [4] 李星, 霍华颂, 时朋朋. 一维六方压电准晶对称条形体中共线双半无限快速传播裂纹的解析解[J]. *固体力学学报*, 2014, 35(02): 135-141. (Li X, Huo H S, Shi P P. Analytic solutions of two collinear fast propagating cracks in a symmetrical strip of one-dimensional hexagonal piezoelectric quasicrystals [J]. *Chinese Journal of Solid Mechanics*, 2014, 35(02): 135-141. (in Chinese))
- [5] Feng X, Fan X Y, Li Y, Zhang H, Zhang L L. Static response and free vibration analysis for cubic quasicrystal laminates with imperfect interfaces[J]. *European Journal of Mechanics-A/Solids*, 2021, 90: 104365.
- [6] Li Y S, Xiao T. Free vibration of the one-dimensional piezoelectric quasicrystal microbeams based on modified couple stress theory[J]. *Applied Mathematical Modelling*, 2021, 96: 733-750.
- [7] Waksmani N, Pan E, Yang L Z, Gao Y. Free vibration of a multilayered one-dimensional quasi-crystal plate[J]. *Journal of Vibration and Acoustics*, 2014, 136(4): 041019.
- [8] 陈韬, 郭俊宏, 田园. 一维六方准晶层合简支梁自由振动与屈曲的精确解[J]. *固体力学学报*, 2023, 44(01): 109-119. (Chen T, Guo J H, Tian Y. Exact solution of free vibration and buckling of one dimensional hexagonal simply-supported and layered quasicrystal beams [J]. *Chinese Journal of Solid Mechanics*, 2023, 44(01): 109-119. (in Chinese))
- [9] 周红梅, 韩康乐, 禹建功, 张会端, 王现辉, 张小明. 压电圆盘的轴对称振动: 改进的双勒让德多项式方法[J]. *振动与冲击*, 2023, 42(21): 169-175. (Zhou H M, Han K L, Yu J G, Zhang H D, Wang X H, Zhang X M. Axis-symmetric vibration of piezoelectric

- disc based on improved double-Legendre polynomial [J]. *Journal of Vibration and Shock*, 2023, 42(21): 169-175. (in Chinese))
- [10] 郭全圆, 刘永刚, 曾奥柯, 闫鹏飞. 螺旋电极压电扭转驱动器的设计与有限元分析[J]. *压电与声光*, 2020, 42(06): 825-830. (Guo Q Y, Liu Y G, Zeng A K, Yan P F. Design and finite element analysis of piezoelectric torsional actuator with spiral electrode [J]. *Piezoelectrics & Acoustooptics*, 2020, 42(06): 825-830. (in Chinese))
- [11] Almeida B V, Pavanello R, Langelaar M. Topology optimization of smart structures with embedded piezoelectric stack actuators using a composite geometry projection method[J]. *Computer Methods in Applied Mechanics and Engineering*, 2024, 429: 117120.
- [12] 王鑫鑫, 禹建功, 张博, 刘灿灿, 王现辉. 一维六方准晶纳米板中 Lamb 波特性研究[J]. *工程力学*, 2023, 40(10): 213-221. (Wang X X, Yu J G, Zhang B, Liu C C, Wang X H. Investigation on Lamb wave characteristics in one-dimensional hexagonal quasicrystal nano plates[J]. *Engineering Mechanics*, 2023, 40(10): 213-221. (in Chinese))
- [13] 禹建功, 王开, 任小强, 王现辉, 张博. 功能梯度压电空心圆柱中分数阶热弹导波的频散和衰减特性[J]. *应用数学和力学*, 2023, 44(11): 1325-1340. (Yu J G, Wang K, Ren X Q, Wang X H, Zhang B. Dispersion and attenuation characteristics of fractional-order thermoelastic guided waves in functionally graded piezoelectric hollow cylinders [J]. *Applied Mathematics and Mechanics*, 2023, 44(11): 1325-1340. (in Chinese))
- [14] 张博, 禹建功, 刘丽娜, 张小明. 压电扇形截面柱体结构中的波动特性研究[J]. *应用基础与工程科学学报*, 2020, 28(05): 1259-1269. (Zhang B, Yu J G, Liu L N, Zhang X M. Wave characteristics in piezoelectric cylindrical structures with sector cross-sections [J]. *Journal of Basic Science and Engineering*, 2020, 28(05): 1259-1269. (in Chinese))
- [15] Ding D H, Yang W G, Hu C Z, Wang R H. Generalized elasticity theory of quasicrystals[J]. *Physical Review. B, Condensed Matter*, 1993, 48(10): 7003-7010.
- [16] Hu C, Wang R, Ding D H. Symmetry groups, physical property tensors, elasticity and dislocations in quasicrystals[J]. *Reports on Progress in Physics*, 2000, 63(1): 1-39.
- [17] Oppenheim A V, Schaffer R W. *Digital Signal Processing*[M]. Englewood Cliffs: Prentice-Hall, 1975.
- [18] 陈骥, 姚俊, 曹久大, 赵晓明, 郭伟. 径向极化压电圆管超声换能器的数值模拟[J]. *应用基础与工程科学学报*, 2016, 24(03): 510-520. (Chen J, Yao J, Cao J D, Zhao X M, Guo W. Numerical simulation of radially polarized piezoelectric cylindrical tube ultrasonic transducers[J]. *Journal of Basic Science and Engineering*, 2016, 24(03): 510-520. (in Chinese))
- [19] Zhou H M, Han K L, Elmaimouni L, Wang X H, Yu J G. Double Legendre polynomial quadrature-free method for axisymmetric vibration of functionally graded piezoelectric circular plates[J]. *Journal of Vibration and Control*, 2023, 30(3-4): 598-615.
- [20] Balandin A, Wang K L. Significant decrease of the lattice thermal conductivity due to phonon confinement in a free-standing semiconductor quantum well [J]. *Physical Review B*, 1998, 58(3): 1544-1549.
- [21] Lubensky T C, Ramaswamy S, Toner J. Hydrodynamics of icosahedral quasicrystals[J]. *Physical Review. B, Condensed Matter*, 1985, 32(11): 7444-7452.
- [22] Katz A, Duneau M. Quasiperiodic patterns with icosahedral symmetry[J]. *Journal de Physique*, 1987, 48(3): 181-196.

Free Vibration of One-Dimensional Hexagonal Piezoelectric Quasi-Crystal Discs

Bo Zhang¹ He Ping¹ Liangjuan Li² Xinxin Wang¹ Jiangong Yu¹ Kangle Han¹

(¹*School of Mechanical and Power Engineering, Henan Polytechnic University, Jiaozuo, 454000*)

(²*School of Mathematics and Information Science, Henan Polytechnic University, Jiaozuo, 454000*)

Abstract Piezoelectric quasi-crystal materials possess excellent piezoelectric and phonon-phason coupling effects, ensuring their promising applications in piezoelectric devices, such as sensors and transducers. The performance of piezoelectric devices is closely related to the vibration characteristics. Therefore, the free vibration characteristics of one-dimensional hexagonal piezoelectric quasi-crystal discs are investigated. First, the dynamic equations of one-dimensional hexagonal piezoelectric quasi-crystal discs are derived in the context of three-dimensional phonon-phason-electro-elastic multifield couplings. The traction-free and short-circuit boundary conditions at the upper and bottom surfaces are incorporated into the constitutive equations by introducing the rectangular window function. The double Legendre orthogonal polynomial method is employed to obtain the solutions. To improve the computational efficiency, the analytical expressions of numerical integrations are derived. The influence of the diameter-height ratio and phonon-phason coupling effect on the resonance frequency is then analyzed. Subsequently, based on the finite element method, a simulation program for the free vibration characteristics of one-dimensional hexagonal piezoelectric quasi-crystal discs is developed for the first time to verify the theoretical calculation results. The partial differential equation (PDE) module in the COMSOL software is utilized to conduct the simulation. It is found that, compared with the traditional double orthogonal polynomial method, the analytical double orthogonal polynomial method significantly improves the computational efficiency, with an improvement rate of up to 99%. Changing the diameter-to-height ratio significantly influences the normalized frequency of the phason modes, and the higher-order modes are more sensitive to the change of the diameter-to-height ratio. The normalized frequencies of phonon modes and phason modes increase with the diameter-to-height ratio (D/H). The increase of phonon-phason coupling coefficients leads to a decrease in the normalized frequencies of phonon modes and phason modes, and its influence on the phason modes is more significant. The obtained results lay a basis for designing and optimizing the piezoelectric quasi-crystal sensors and transducers with excellent performance.

Key words piezoelectric quasi-crystal, analytical integration, double Legendre orthogonal polynomial method, free vibration, phonon-phason coupling

附 录

式(17)中出现的矩阵,其具体内容如下所示:

以 A_1 矩阵为例,迭代阵满足如下形式:

$$A1_{nmij} = \begin{bmatrix} A1_{0000} & \cdots & A1_{0N00} & A1_{1000} & \cdots & A1_{1N00} & \cdots & A1_{M000} & \cdots & A1_{MN00} \\ \vdots & \vdots & \vdots & \vdots & \vdots & \vdots & \vdots & \vdots & \vdots & \vdots \\ A1_{000N} & \cdots & A1_{0N0N} & A1_{100N} & \cdots & A1_{1N0N} & \cdots & A1_{M00N} & \cdots & A1_{MN0N} \\ A1_{0010} & \cdots & A1_{0N10} & A1_{1010} & \cdots & A1_{1N10} & \cdots & A1_{M010} & \cdots & A1_{MN10} \\ \vdots & \vdots & \vdots & \vdots & \vdots & \vdots & \vdots & \vdots & \vdots & \vdots \\ \vdots & \vdots & \vdots & \vdots & \vdots & \vdots & \vdots & \vdots & \vdots & \vdots \\ A1_{001N} & \cdots & A1_{0N1N} & A1_{101N} & \cdots & A1_{1N1N} & \cdots & A1_{M01N} & \cdots & A1_{MN1N} \\ \vdots & \vdots & \vdots & \vdots & \vdots & \vdots & \vdots & \vdots & \vdots & \vdots \\ A1_{00M0} & \cdots & A1_{0NM0} & A1_{10M0} & \cdots & A1_{1NM0} & \cdots & A1_{M0M0} & \cdots & A1_{MNM0} \\ \vdots & \vdots & \vdots & \vdots & \vdots & \vdots & \vdots & \vdots & \vdots & \vdots \\ A1_{00MN} & \cdots & A1_{0NMN} & A1_{10MN} & \cdots & A1_{1NMN} & \cdots & A1_{M0MN} & \cdots & A1_{MNMN} \end{bmatrix}$$

其中：

$$A1_{nmij} = C_{11} \times u[m, n, 2, 0, i, j, 2, 0] + C_{12} \times u[m, n, 1, 0, i, j, 1, 0] + C_{11} \times ky[m, n, 2, 0, i, j, 1, 0] + C_{12} \times ky[m, n, 1, 0, i, j, 0, 0] + C_{44} \times u[m, n, 2, 0, i, j, 0, 2] + C_{44} \times kz[m, n, 2, 0, i, j, 0, 1] + C_{11} \times u[m, n, 1, 0, i, j, 1, 0] - C_{11} \times u[m, n, 0, 0, i, j, 0, 0] - C_{12} \times u[m, n, 1, 0, i, j, 1, 0]$$

过程矩阵 $A1, A2, A3, A4, B1, B2, B3, B4, C1, C2, C3, C4, D1, D2, D3, D4, M1, M2, M3$ 的形式同上，

其中：

$$A2_{nmij} = C_{13} \times u[m, n, 2, 0, i, j, 1, 1] + C_{44} \times u[m, n, 2, 0, i, j, 1, 1] + C_{13} \times ky[m, n, 2, 0, i, j, 0, 1] + C_{44} \times kz[m, n, 2, 0, i, j, 1, 0]$$

$$A3_{nmij} = R1 \times u[m, n, 2, 0, i, j, 1, 1] + R1 \times ky[m, n, 2, 0, i, j, 0, 1] + R3 \times u[m, n, 2, 0, i, j, 1, 1] + R3 \times kz[m, n, 2, 0, i, j, 1, 0]$$

$$A4_{nmij} = e_{31} \times (2 \times u[m, n, 2, 1, i, j, 1, 0] - H \times u[m, n, 2, 0, i, j, 1, 0] + u[m, n, 2, 2, i, j, 1, 1] - H \times u[m, n, 2, 1, i, j, 1, 1]) + e_{31} \times (2 \times ky[m, n, 2, 1, i, j, 0, 0] - H \times ky[m, n, 2, 0, i, j, 0, 0] + ky[m, n, 2, 2, i, j, 0, 1] - H \times ky[m, n, 2, 1, i, j, 0, 1]) + e_{15} \times (2 \times u[m, n, 2, 1, i, j, 1, 0] - H \times u[m, n, 2, 0, i, j, 1, 0] + u[m, n, 2, 2, i, j, 1, 1] - H \times u[m, n, 2, 1, i, j, 1, 1]) + e_{15} \times (kz[m, n, 2, 2, i, j, 1, 0] - H \times kz[m, n, 2, 1, i, j, 1, 0])$$

$$B1_{nmij} = C_{44} \times u[m, n, 1, 0, i, j, 1, 1] + C_{44} \times ky[m, n, 1, 0, i, j, 0, 1] + C_{13} \times u[m, n, 1, 0, i, j, 1, 1] + C_{13} \times u[m, n, 0, 0, i, j, 0, 1] + C_{13} \times kz[m, n, 1, 0, i, j, 1, 0] + C_{13} \times kz[m, n, 0, 0, i, j, 0, 0] + C_{44} \times u[m, n, 0, 0, i, j, 0, 1]$$

$$B2_{nmij} = C_{44} \times u[m, n, 1, 0, i, j, 2, 0] + C_{44} \times ky[m, n, 1, 0, i, j, 1, 0] + C_{33} \times u[m, n, 1, 0, i, j, 0, 2] + C_{33} \times kz[m, n, 1, 0, i, j, 0, 1] + C_{44} \times u[m, n, 0, 0, i, j, 1, 0]$$

$$B3_{nmij} = R_3 \times u[m, n, 1, 0, i, j, 2, 0] + R_3 \times ky[m, n, 1, 0, i, j, 1, 0] + R_2 \times u[m, n, 1, 0, i, j, 0, 2] + R_2 \times kz[m, n, 1, 0, i, j, 0, 1] + R3 \times u[m, n, 0, 0, i, j, 1, 0]$$

$$B4_{nmij} = e_{15} \times (u[m, n, 1, 2, i, j, 2, 0] - H \times u[m, n, 1, 1, i, j, 2, 0]) + e_{15} \times (ky[m, n, 1, 2, i, j, 1, 0] - H \times ky[m, n, 1, 1, i, j, 1, 0]) + e_{33} \times (2 \times u[m, n, 1, 0, i, j, 0, 0] + 4 \times u[m, n, 1, 1, i, j, 0, 1] - 2 \times H \times u[m, n, 1, 0, i, j, 0, 1] + u[m, n, 1, 2, i, j, 0, 2] - H \times u[m, n, 1, 1, i, j, 0, 2]) + e_{33} \times (2 \times kz[m, n, 1, 1, i, j, 0, 0] - H \times kz[m, n, 1, 0, i, j, 0, 0] + kz[m, n, 1, 2, i, j, 0, 1] - H \times kz[m, n, 1, 1, i, j, 0, 1]) + e_{15} \times (u[m, n, 0, 2, i, j, 1, 0] - H \times u[m, n, 0, 1, i, j, 1, 0])$$

$$C1_{nmij} = R_3 \times u[m, n, 1, 0, i, j, 1, 1] + R_3 \times ky[m, n, 1, 0, i, j, 0, 1] + R_1 \times u[m, n, 1, 0, i, j, 1, 1] + R_1 \times u[m, n, 0, 0, i, j, 0, 1] + R_1 \times kz[m, n, 1, 0, i, j, 1, 0] + R_1 \times kz[m, n, 0, 0, i, j, 0, 0] +$$

$$R_3 \times u[m, n, 0, 0, i, j, 0, 1]$$

$$C2_{nmij} = R_3 \times u[m, n, 1, 0, i, j, 2, 0] + R_3 \times ky[m, n, 1, 0, i, j, 1, 0] + R_2 \times u[m, n, 1, 0, i, j, 0, 2] + R_2 \times kz[m, n, 1, 0, i, j, 0, 1] + R_3 \times u[m, n, 0, 0, i, j, 1, 0]$$

$$C3_{nmij} = K_2 \times u[m, n, 1, 0, i, j, 2, 0] + K_2 \times ky[m, n, 1, 0, i, j, 1, 0] + K_1 \times u[m, n, 1, 0, i, j, 0, 2] + K_1 \times kz[m, n, 1, 0, i, j, 0, 1] + K_2 \times u[m, n, 0, 0, i, j, 1, 0]$$

$$C4_{nmij} = d_{15} \times (u[m, n, 1, 2, i, j, 2, 0] - H \times u[m, n, 1, 1, i, j, 2, 0]) + d_{15} \times (ky[m, n, 1, 2, i, j, 1, 0] - H \times ky[m, n, 1, 1, i, j, 1, 0]) + d_{33} \times (2 \times u[m, n, 1, 0, i, j, 0, 0] + 4 \times u[m, n, 1, 1, i, j, 0, 1] - 2 \times H \times u[m, n, 1, 0, i, j, 0, 1] + u[m, n, 1, 2, i, j, 0, 2] - H \times u[m, n, 1, 1, i, j, 0, 2]) + d_{33} \times (2 \times kz[m, n, 1, 1, i, j, 0, 0] - H \times kz[m, n, 1, 0, i, j, 0, 0] + kz[m, n, 1, 2, i, j, 0, 1] - H \times kz[m, n, 1, 1, i, j, 0, 1]) + d_{15} \times (u[m, n, 0, 2, i, j, 1, 0] - H \times u[m, n, 0, 1, i, j, 1, 0])$$

$$D1_{nmij} = e_{15} \times u[m, n, 1, 0, i, j, 1, 1] + e_{15} \times ky[m, n, 1, 0, i, j, 0, 1] + e_{31} \times u[m, n, 1, 0, i, j, 1, 1] + e_{31} \times u[m, n, 0, 0, i, j, 0, 1] + e_{15} \times u[m, n, 0, 0, i, j, 0, 1]$$

$$D2_{nmij} = e_{15} \times u[m, n, 1, 0, i, j, 2, 0] + e_{15} \times ky[m, n, 1, 0, i, j, 1, 0] + e_{33} \times u[m, n, 1, 0, i, j, 0, 2] + e_{15} \times u[m, n, 0, 0, i, j, 1, 0]$$

$$D3_{nmij} = d_{15} \times u[m, n, 1, 0, i, j, 2, 0] + d_{15} \times ky[m, n, 1, 0, i, j, 1, 0] + d_{33} \times u[m, n, 1, 0, i, j, 0, 2] + d_{15} \times u[m, n, 0, 0, i, j, 1, 0]$$

$$D4_{nmij} = -\delta_{11} \times (u[m, n, 1, 2, i, j, 2, 0] - H \times u[m, n, 1, 1, i, j, 2, 0]) - \delta_{11} \times (ky[m, n, 1, 2, i, j, 1, 0] - H \times ky[m, n, 1, 1, i, j, 1, 0]) - \delta_{33} \times (2 \times u[m, n, 1, 0, i, j, 0, 0] + 4 \times u[m, n, 1, 1, i, j, 0, 1] - 2 \times H \times u[m, n, 1, 0, i, j, 0, 1] + u[m, n, 1, 2, i, j, 0, 2] - H \times u[m, n, 1, 1, i, j, 0, 2]) - \delta_{11} \times (u[m, n, 0, 2, i, j, 1, 0] - H \times u[m, n, 0, 1, i, j, 1, 0])$$

$$M1_{nmij} = -\rho \times u[m, n, 2, 0, i, j, 0, 0]$$

$$M2_{nmij} = -\rho \times u[m, n, 1, 0, i, j, 0, 0]$$

$$M3_{nmij} = -\rho \times u[m, n, 1, 0, i, j, 0, 0]$$

$$u[m_-, n_-, o_-, p_-, i_-, j_-, k_-, l_-] = \int_0^R \int_0^H \pi_1(r) \pi_3(z) \times Q_m(r) \times Q_n(z) \times r^o \times z^p \times \frac{\partial^k Q_i}{\partial r^k} \times \frac{\partial^l Q_j}{\partial r^l} dr dz$$

$$ky[m_-, n_-, o_-, p_-, i_-, j_-, k_-, l_-] = \int_0^R \int_0^H \frac{\partial \pi_1(r)}{\partial r} \pi_3(z) \times Q_m(r) \times Q_n(z) \times r^o \times z^p \times \frac{\partial^k Q_i}{\partial r^k} \times \frac{\partial^l Q_j}{\partial r^l} dr dz$$

$$kz[m_-, n_-, o_-, p_-, i_-, j_-, k_-, l_-] = \int_0^R \int_0^H \pi_1(r) \frac{\partial \pi_3(z)}{\partial z} \times Q_m(r) \times Q_n(z) \times r^o \times z^p \times \frac{\partial^k Q_i}{\partial r^k} \times \frac{\partial^l Q_j}{\partial r^l} dr dz$$